Growth of $Ba_xSr_{1-x}SO_4$ nano-steps on barite (0 0 1) face

Chen YuHang [a], Agustina Asenjo [b], Nuria Sánchez-Pastor [c], Lurdes Fernández-Díaz [c], Julio Gómez [a], Carlos M. Pina [c,*]

[a] *Dpto. Física de la Materia Condensada, Universidad Autónoma de Madrid, 28049 Madrid, Spain*
[b] *Instituto de Ciencia de Materiales de Madrid, CSIC. Cantoblanco, 28049 Madrid, Spain*
[c] *Dpto. Cristalografía y Mineralogía, Universidad Complutense de Madrid, 28040 Madrid, Spain*

Abstract

Crystal growth has been promoted in the fluid cell of an Atomic Force Microscope (AFM) by passing Ba–Sr–SO_4 aqueous solutions over barite (0 0 1) cleavage surfaces. Steps advance in structural continuity with the original barite (0 0 1) surfaces and two-dimensional nucleation occurs preferentially on the newly-formed terraces. The terraces are, on average, 7.5% lower than pure barite terraces. Since the ionic radius of Sr^{2+} is smaller that the ionic radius of Ba^{2+}, the reduction of terrace height is consistent with an extensive incorporation of Sr^{2+} into the barite structure. Therefore, it can be considered that the newly-formed terraces have compositions corresponding to terms of the $Ba_xSr_{1-x}SO_4$ solid solution. A non-linear dependence of step rate on [$SrSO_4$] concentration in the solution (and therefore on supersaturation) has been found. The growth behaviour has been discussed by considering both the physicochemical properties of the $Ba_xSr_{1-x}SO_4$ solid solution–aqueous solution (SS–AS) system and a kinetic-based step growth model.

Keywords: Atomic force microscopy; Barite; Celestite; Solid solution; Crystal growth

1. Introduction

In the last two decades, Atomic Force Microscopy (AFM) has been used to investigate monostep growth kinetics on surfaces of numerous mineral and synthetic compounds because of two reasons: the unprecedented ability to obtain high resolution images on insulators and its versatility to work in different environments, including ionic solutions [1–7]. In situ AFM growth experiments have allowed to determine monostep motion dependencies on supersaturation, as well as to obtain information about kink dynamics in pure substances [8–12]. A number of experimental works have also approached the study of the effect of some foreign ions on growth kinetics assuming that these ions are impurities that disrupt the "normal" motion of monosteps [13–16]. However, this approach is not entirely justified when foreign ions incorporate into the crystal structure forming extent solid solutions. In such a case, these ions can hardly be considered as impurities.

Recent AFM observations of mineral surfaces growing from aqueous solutions containing divalent cations that can be extensively incorporated into crystal structures (e.g. Mg^{2+}, Mn^{2+} and Sr^{2+} in calcite; Sr^{2+} in barite [17 and references therein]) revealed that classical impurity models (i.e. isomorphic impurity incorporation model [15,18,19] and step-pinning model [20–24]) fail to explain all the aspects of the monostep growth kinetics. In particular, the different growth rates of the first monolayers compared to successive layers and the increase of growth rates with the increase of the "impurity" concentration challenge the classical models. Several authors have pointed out that changes in crystal solubility or even a

* Corresponding author. Tel.: +34 913944879; fax: +34 913944872.
E-mail addresses: chenyh@mail.ustc.edu.cn (C. YuHang), aasenjo@icmm.csic.es (A. Asenjo), nsanchez@geo.ucm.es (N. Sánchez-Pastor), lfdiaz@geo.ucm.es (L. Fernández-Díaz), julio.gomez@uam.es (J. Gómez), cmpina@geo.ucm.es (C.M. Pina).

"non yet characterised kinetic" effect could be cause for the observed anomalous monostep growth kinetics [25]. Other authors, instead, suggest that the modification of the physicochemical properties of the substrate when cations are incorporated into the first monolayers (e.g. generation of an inhomogeneous surface strain) can strongly influence the growth behaviour of subsequent monolayers [6]. In any case, when the cations that modified the step kinetics incorporate in high amounts into the crystal structures, it seems reasonable to approach the problem of monostep motion by considering the chemical composition of both the solution and the growing crystal as variables. This approach requires a detailed knowledge of the physicochemical and thermodynamical properties of the solid solution–aqueous solution (SS–AS) systems.

In this work we present new in situ AFM observations of growth on barite. Step growth was promoted by passing Ba–Sr–SO_4 aqueous solutions over barite (●●1) cleavage surfaces. These steps have been considered as $Ba_xSr_{1-x}SO_4$ solid solution steps propagating on the barite (001) surface. The observed non-linear step kinetics has been discussed on the basis of the SS–AS theory [26–29] and a kinetic-based step growth model.

2. The $Ba_xSr_{1-x}SO_4$–H_2O SS–AS system: theoretical background

The barite (●●1) face has been revealed as a suitable substrate to explore the growth behaviour on a nanoscale of both the end-members (celestite and barite) and intermediate compositions of the $Ba_xSr_{1-x}SO_4$ solid solution [2,7,12,29–33]. Barite ($BaSO_4$) and celestite ($SrSO_4$) are isostructural and they crystallise in the orthorhombic *Pnma* space group. The cell parameters are $a_0 = 8.884$Å, $b_● = 5.455$ Å and $c_● = 7.156$ Å for barite, and $a_0 = 8.389$ Å, $b_0 = 5.365$ Å and $c_● = 6.885$ Å for celestite [34,35].

The compositional equilibrium relationships between the solid and the aqueous phases in the $Ba_xSr_{1-x}SO_4$–H_2O SS–AS system can be described by means of the Lippmann model [26–28,36]. Fig. 1 shows the Lippmann diagram for the $Ba_xSr_{1-x}SO_4$–H_2O SS–AS system, in which the solid and aqueous phase compositions are represented by the so-called *solidus* and *solutus* curves, which express the total solubility product, $\Sigma\Pi$ (i.e. the sum of the partial solubility products contributed by the individual end-members of the solid solution), as a function of the solid and aqueous compositions, respectively. The Lippmann diagram for the $Ba_xSr_{1-x}SO_4$–H_2O SS–AS system has been constructed by assuming that the $Ba_xSr_{1-x}SO_4$ solid solution is continuous and ideal. Although the degree of ideality of the $Ba_xSr_{1-x}SO_4$ solid solution is still controversial [37–41], the high difference in solubility products of the end members at 25 °C: $K_{BaS●_4} = 10^{-9.98}$ for barite [42] and $K_{SrS●_4} = 10^{-6.63}$ for celestite [43] seems to be the main factor controlling its nucleation and growth behaviour [28,44]. The extremely low solubility of barite compared with celestite determines

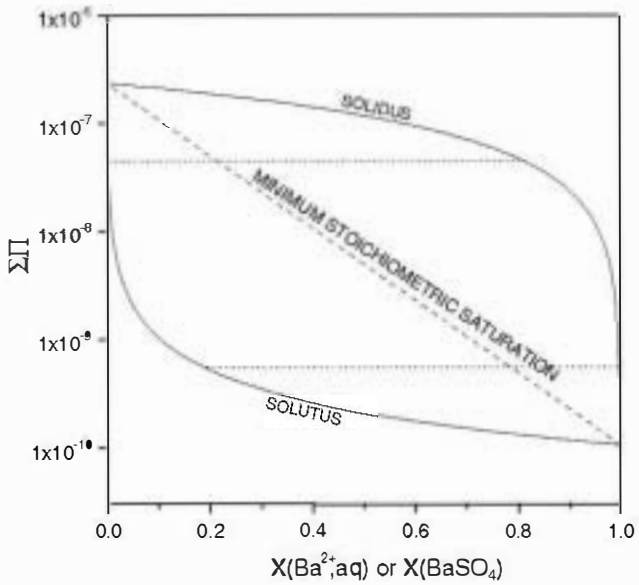

Fig. 1. Lippmann diagram for the $Ba_xSr_{1-x}SO_4$ H_2O SS AS system at 25 °C drawn assuming
curves are represented on the ordinate versus $X_{BaS●_4}$ and $X_{Ba,aq}$ on the abscissa, respectively. The tie-lines shown in the diagram connect two solids mole fractions with their corresponding aqueous activity fractions at thermodynamic equilibrium. The dashed line represents the minimum stoichiometric saturation of the $Ba_xSr_{1-x}SO_4$ solid solution.

that the *solutus* and *solidus* curves plot very far apart in the Lippmann diagram, so that extremely Sr-poor solid solutions are in equilibrium with Sr-rich aqueous solutions. Therefore, from the point of view of the equilibrium thermodynamics, to precipitate Sr-rich solid solutions, the aqueous phase must be extremely Ba-poor.

On the basis of the Lippmann model it is possible to derive expressions which describe the supersaturation of a given aqueous solution with respect to the whole range of solid solution compositions [28,45]. The so-called stoichiometric supersaturation, $\beta(x)$, is the simplest expression for calculating supersaturations for SS–AS systems. This expression is based on the concept of the minimum stoichiometric saturation constant, i.e. a straightforward generalisation of the solubility product to the case of SS–AS systems [27]. In the case of the $Ba_xSr_{1-x}SO_4$–H_2O SS–AS system, the minimum stoichiometric saturation constant is given by the expression:

$$K_{ss} = (K_{SrS●_4} X_{SrS●_4} \gamma_{SrS●_4})^{1-x} (K_{BaSO_4} X_{BaS●_4} \gamma_{BaS●_4})^{x} \qquad (1)$$

where $x = X_{BaS●_4}$ and $1 - x = X_{SrSO_4}$, and $\gamma_{BaS●_4}$ and $\gamma_{SrS●_4}$ are the molar fractions and the activity coefficients of $BaSO_4$ and $SrSO_4$ in the solid solution, respectively. Stoichiometric saturations for each possible solid solution composition can also be represented on a Lippmann diagram. These stoichiometric saturation curves have a characteristic minimum $\Sigma\Pi$ value, i.e. the minimum stoichiometric saturation point [27]. For the $Ba_xSr_{1-x}SO_4$–H_2O SS–AS system, a minimum stoichiometric saturation curve has been constructed from the series of minimum stoichiometric saturation points (dashed line in Fig. 1).

By considering Eq. (1) as the equilibrium state of reference, the stoichiometric supersaturation of an aqueous solution with respect to the whole range of compositions of the $Ba_xSr_{1-x}SO_4$ solid solution can be expressed by

$$\beta(x) = \frac{a(Sr^{2+})^{1-x}a(Ba^{2+})^{x}a(SO_4^{2-})}{(K_{SrSO_4}\cdot X_{SrSO_4}\gamma_{SrSO_4})^{1-x}(K_{BaSO_4}\cdot X_{BaSO_4}\gamma_{BaSO_4})^{x}} \quad (2)$$

where $a(Sr^{2+})$, $a(Ba^{2+})$ and $a(SO_4^{2-})$ are the activities of the ions in the aqueous phase.

Eq. (2) implies that for a given aqueous solution composition, supersaturation is different for different compositions of the solid solution, i.e. in the case of SS–AS systems, supersaturation is not a single value but a function of the solid solution composition. Since crystal growth kinetics is strongly determined by supersaturation, this means that different compositions of a solid solution can grow simultaneously at different rates (or even according to different growth mechanisms) from the same aqueous solution [29].

3. Experimental procedure

Nanoscale observations of growth on barite were conducted with an Atomic Force Microscope (AFM) equipped with a fluid cell (Nanotec Electronica S.L.) Optically clear barite crystals were cleaved on (001) faces prior each experiment and placed in the fluid cell of the AFM. In order to promote growth, Ba–Sr–SO_4 aqueous solutions with different Ba/Sr ratios were passed over barite (001) surfaces (see Table 1). A constant flow rate of 10 μl/min was used to avoid solution/sample equilibrium. Growth solutions were prepared from $BaCl_2$, $SrCl_2$ and Na_2SO_4 reagent grade using deionised water. The activities for the Ba^{2+}, Sr^{2+} and SO_4^{2-} ions were calculated using the program PHREEQC [46]. Sequences of AFM cantilever deflection images (error signal) were taken in order to measure the growth velocity of steps on barite (001) face. AFM topographic images were taken to measure the height of steps and two-dimensional islands grown from solutions with different [$SrSO_4$] concentrations. All the images shown in this work were taken in constant force mode. Silicon nitride (Olympus OMCL-HA100WS) tips with a nominal force constant $k = 15$ N/m were used. In most of our experiments, the tip scans the surface at 38 microns/s. All the experiments were conducted at room temperature.

4. Results

AFM images of freshly cleaved barite (001) faces invariably show flat terraces separated by steps one unit cell in height, i.e. 7.15 Å [2,12,30–32]. These steps are usually parallel to ⟨100⟩, ⟨120⟩ and ⟨110⟩ crystallographic directions [7]. When solutions bearing Sr^{2+}, Ba^{2+} and SO_4^{2-} with the concentrations listed in Table 1 (experiment numbers 1–8) are passed over barite (001) surfaces, step advancement was observed. Growth steps have half a unit cell in height (~3.5 Å) and their rate of advancement is highly anisotropic, with reversed fast and slow directions occurring in successive growth monolayers. As a result, once a fast monostep meets a slow monostep the rate at which the double step (~7 Å) propagates on the surface is approximately equal to the step rate of a slow monostep. In this work, we have measured growth rates of double monosteps parallel to ⟨120⟩ directions. In some cases, rates of double steps parallel to other directions (e.g. ⟨100⟩ and ⟨110⟩) have been also measured. However, since step rates of all slow steps on barite (001) are very similar, such measurements can be also considered equivalent to step growth rates along ⟨120⟩ direction.

The spreading of double steps on barite (001) generates new terraces (one unit cell in height) in structural continuity with the initial terraces (see Fig. 2). Both height and deflection images show a slight contrast between the original step edge and the newly-grown terrace. This contrast is more marked as the [$SrSO_4$] concentration increases in the growth aqueous solution. Fig. 3 shows the variation of the height of the newly-grown terraces with the [$SrSO_4$] concentration of the aqueous solution. These measurements indicate that the height of newly-grown steps is, on average, 7.5% lower than the original barite cleavage steps.

Another interesting microtopographic feature observed during the AFM growth experiments is the formation of two-dimensional nuclei (hereafter referred as two-dimensional islands). Two-dimensional islands are not

Table 1
Concentrations and ionic activities of the solutions used in the AFM experiments

Experiment number	Solution composition					
	$SrCl_2$ (μmol/l)	$BaCl_2$ (μmol/l)	Na_2SO_4 (μmol/l)	$a(Sr^{2+})$	$a(Ba^{2+})$	$a(SO_4^{2-})$
1	900	1	900	6.15×10^{-4}	6.05×10^{-7}	6.08×10^{-4}
2	1000	1	1000	6.70×10^{-4}	5.88×10^{-7}	6.62×10^{-4}
3	1050	1	1050	6.97×10^{-4}	5.81×10^{-7}	6.89×10^{-4}
4	1100	1	1100	7.24×10^{-4}	5.73×10^{-7}	7.14×10^{-4}
5	1150	1	1150	7.50×10^{-4}	5.66×10^{-7}	7.40×10^{-4}
6	1175	1	1175	7.63×10^{-4}	5.63×10^{-7}	7.53×10^{-4}
7	1225	1	1225	7.89×10^{-4}	5.57×10^{-7}	7.79×10^{-4}
8	1250	1	1250	8.01×10^{-4}	5.53×10^{-7}	7.90×10^{-4}
9	1050		1050	6.97×10^{-4}		6.89×10^{-4}
10	1250		1250	8.01×10^{-4}		7.90×10^{-4}

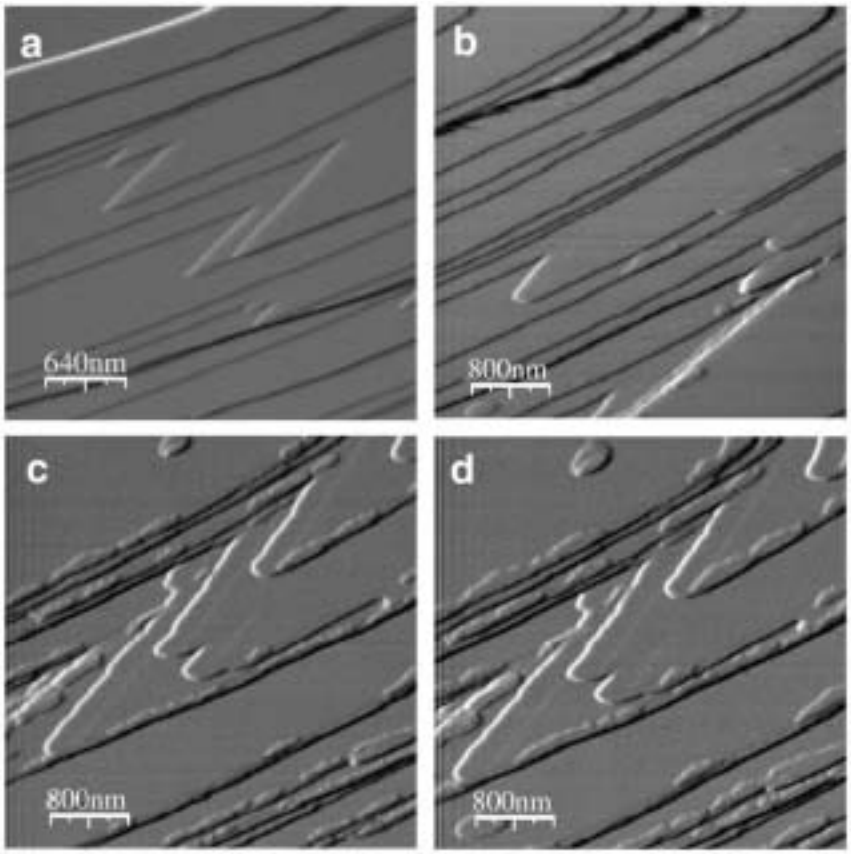

Fig. 2. Growth sequence showing the advancement of steps with general composition $Ba_xSr_{1-x}SO_4$ on a barite (001) surface. The concentration of the aqueous solution was: $a(Sr^{2+}) = 6.97 \times 10^{-4}$, $a(SO_4^{2-}) = 6.89 \times 10^{-4}$ and $a(Ba^{2+}) = 5.81 \times 10^{-7}$ (solution 3 in Table 1). (a) original surface with cleavage steps. (b–d) advancement of steps one-unit-cell in height. Note the slight difference in contrast that allows to distinguish the original step edges. Along the interfaces between the initial cleavage step edges and the newly-grown terraces is frequent to observe the formation of two-dimensional islands (~3.5 Å in height). The AFM images were taken in contact mode and displaying the cantilever deflection signal.

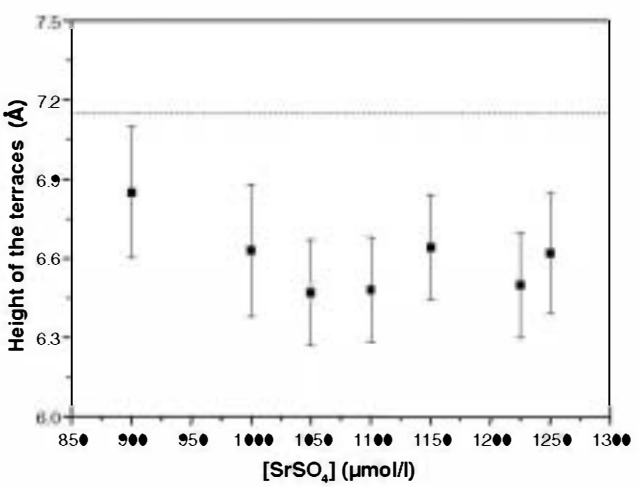

Fig. 3. Height of the newly-grown one-unit-cell terraces (advancement of double steps) versus the $[SrSO_4]$ concentration of the aqueous solution. The horizontal dashed line indicates the height of a pure barite cleavage step (7.15 Å) as a reference.

homogeneously distributed on the barite (001) surfaces, but they preferentially form along the interfaces between the original cleavage step edges and the newly-grown terraces (see Fig. 4). The shape of the islands is similar to the typical shape reported for barite and celestite in previous works, i.e., with two straight edges and a curved one [30,31]. However, once these islands appear on the terrace interfaces, the subsequent growth is clearly anisotropic: the two-dimensional islands grow faster on the newly-grown terraces (see Fig. 4).

Two-dimensional islands are half unit cell in height. The plot in Fig. 5 shows the height of two-dimensional islands versus the $[SrSO_4]$ concentration of the aqueous solutions. As in the case of the newly-grown terraces, the height of the islands is smaller than the height corresponding to pure barite two-dimensional islands (horizontal reference line at 3.5 Å in Fig. 5). Although there is not a systematic variation of the islands height with the $[SrSO_4]$ concentration in the solution, we have observed that islands which had grown on previously formed islands were slightly higher than the islands of the "first generation".

The clear difference in contrast between the newly-grown and the original barite (001) terraces allowed us to measure the advancement of growth double steps with time. As can be seen in Fig. 6, in all the cases (experiments 1–8) such advancements are linear functions of time. The growth rate of the steps was determined from the slopes of the lines fitted to the experimental data. Fig. 7 shows

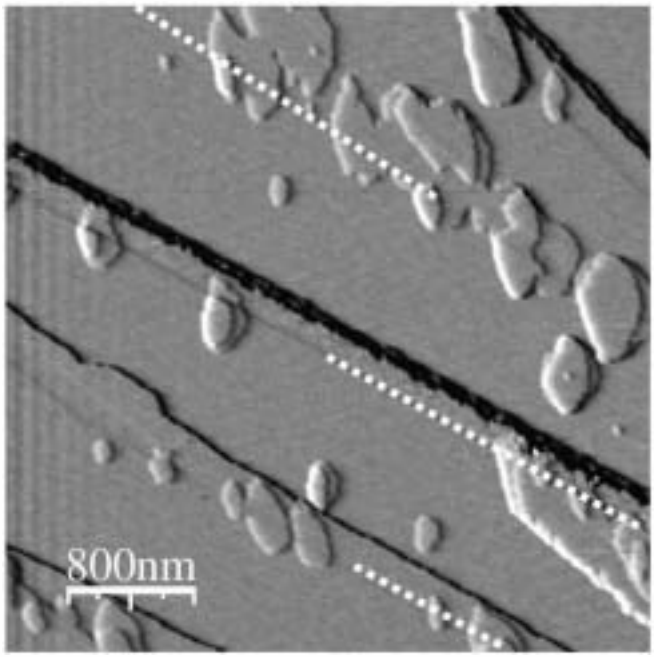

Fig. 4. AFM deflection image showing two-dimensional islands decorating the newly-grown terraces. The concentration of the aqueous solution was: $a(Sr^{2+}) = 6.70 \times 10^{-4}$, $a(SO_4^{2-}) = 6.62 \times 10^{-4}$ and $a(Ba^{2+}) = 5.88 \times 10^{-7}$ (solution 2 in Table 1). On the picture the growth anisotropy can be clearly appreciated, i.e. the islands spread faster on the newly-grown terraces than on the original barite terraces. Dotted lines indicate the position of the initial barite step edges.

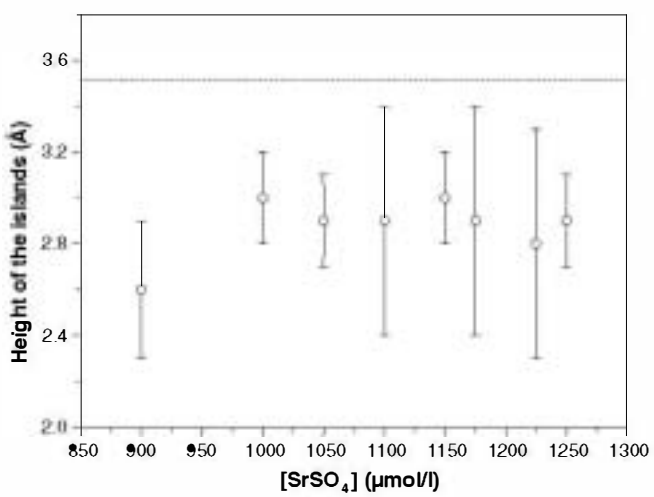

Fig. 5. Height of the islands (half a unit cell) versus the $[SrSO_4]$ concentration in the growth aqueous solution. The reference horizontal line indicates the height of a pure barite island (3.5 Å).

the growth rates of the steps which have grown from solutions with increasing $[SrSO_4]$ concentration. Steps growth rates are lower than 0.06 nm/s for solutions with $[SrSO_4]$ concentrations under 1150 μmol/l (solutions 1–5). For higher $[SrSO_4]$ concentrations (solutions 6–8), growth rates increase rapidly. The maximum growth rate measured was 0.41 nm/s (solution 8). When solutions with $[SrSO_4]$ concentration higher than 1250 μmol/l were used, growth is

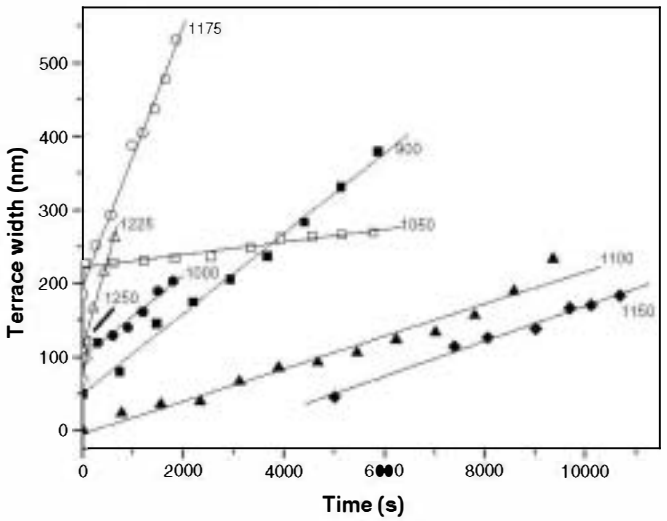

Fig. 6. Terrace width versus time. Numbers indicate the $[SrSO_4]$ concentration of the solutions in μmol/l. In all the experiments, the terrace advancement is a linear function of time.

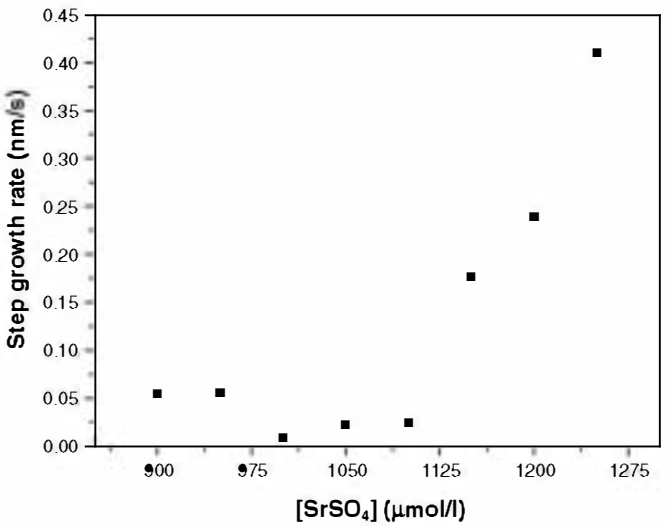

Fig. 7. Growth rates of $Ba_xSr_{1-x}SO_4$ steps on barite (001) face versus $[SrSO_4]$ concentration in the aqueous solution. These values have been obtained from the slopes of the lines fitted to the experimental data in Fig. 6.

so fast that the measurement of growth rates from AFM images is extremely difficult.

Two additional growth AFM experiments were conducted using solutions with $[SrSO_4]$ concentrations of 1050 μmol/l and 1250 μmol/l, but without containing Ba (experiments 9 and 10). In both cases no growth was observed for periods of time longer than 2 h.

5. Discussion

5.1. Growth of the $Ba_xSr_{1-x}SO_4$ solid solution on barite (001) face

AFM observations presented in the previous section demonstrate that cleavage ⟨120⟩ steps on barite (001)

surface are able to grow from Ba–Sr–SO_4 aqueous solutions with Ba/Sr ratios higher than 0.0008. These growth steps are double, formed by two half unit cell steps, i.e. the thickness of the elementary growth layer for barite (001) face according to the PBC theory (~3.5 Å in height) [47,48]. As we mention in Section 4, due to the high anisotropy of growth of the steps on barite (001) faces [12,31,32] the advancement of double steps is limited by the slowest monosteps. Therefore, our advancement rate measurements approximately correspond to the velocity of the slowest elementary growth ⟨120⟩ steps on barite (001) face.

As was shown in Figs. 2 and 4, the step advancement leads to the formation of new terraces in structural continuity with the original barite cleavage terraces. The most remarkable feature of the newly-grown terraces is that they are, on average, 7.5 % lower than the original barite cleavage terraces. Since the ionic radius of Sr^{2+} (1.31 Å) is smaller than the ionic radius of Ba^{2+}(1.47 Å), such a decrease in terrace height can be attributed to the incorporation of the Sr^{2+} ion into the barite structure during growth. Moreover, in the 900 μmol/l < [$SrSO_4$] < 1150 μmol/l concentration range, the reduction in terrace height depends on the [$SrSO_4$] concentration in the aqueous solution: the higher the concentration the lower the terrace. Therefore, the Sr^{2+} incorporation can be considered to occur isomorphically and, consequently, the observed growth corresponds to the advancement of steps of the $Ba_xSr_{1-x}SO_4$ solid solution on the barite (001) surface.

Although the decrease in terrace height can be clearly related to the Sr^{2+} incorporation during growth, such a decrease is higher than expected for the substitution of Ba^{2+} by the smaller Sr^{2+} ion in the barite structure. For the extreme case of newly-grown terraces formed of pure $SrSO_4$, they should have a height of 6.85 Å, i.e. a reduction of a 3.9% with respect to a pure $BaSO_4$ terrace. In contrast, our height measurements indicate reductions ranging from 4.2% to 9.4% in the c parameter with respect to a pure $BaSO_4$ terrace, which are too high even considering the measurement error. This reduction suggests a relaxation of the structure of the newly-grown terraces, presumably as a consequence of the accommodation of the strain generated by the difference in chemical composition. If we consider a hypothetical perfect match between a pure $SrSO_4$ monolayer and the barite (001) substrate, in order to maintain constant the volume of the $SrSO_4$ unit cell, a reduction of an 11.9% in the length of the c axis compared to pure barite is required. This value is consistent with our measurements, indicating both that Sr^{2+} widely incorporates into the barite structure and that the structure of the newly-grown layer relaxes on the barite (001) substrate. Since the relationship between composition, relaxation and height of terraces is difficult to evaluate (and beyond the scope of this work), our height measurements have not been used to estimate the actual composition of the $Ba_xSr_{1-x}SO_4$ terraces. This could be done in the future by assuming that, once the effect of relaxation is corrected, the lattice parameters and, in particular the c parameter of the $Ba_xSr_{1-x}SO_4$ solid solution, vary linearly with the Ba/Sr ratio in the crystal.

The observation of two-dimensional islands preferentially on newly-grown terraces is also consistent with the formation of a Sr-rich substrate. The formation of Sr-rich two-dimensional islands on a Sr-rich substrate would be favoured as a result of the lower mismatch between parallel directions through the interface when the compositional differences are minimised. As a consequence, a lower structural relaxation on the (001) plane is required and, therefore, the length reduction along c axis is lower. This is in agreement with our AFM measurements of the height of two-dimensional islands.

5.2. *Growth kinetics of $Ba_xSr_{1-x}SO_4$ nano-steps*

AFM measurements show that for solutions with [$SrSO_4$] concentrations below 1150 μmol/l (solutions 1–5), step velocities on barite (001) are low and weakly dependent on the [$SrSO_4$] concentration (<0.06 nm/s). In contrast, for solutions with [$SrSO_4$] concentrations above 1150 μmol/l (solutions 6–8), step velocities rapidly increases with the Sr content in the solution (from 0.17 nm/s to 0.41 nm/s). As it was shown in Section 5.1, the decrease in step heights as the [$SrSO_4$] concentration in the solution increases indicates that Sr^{2+} extensively incorporates in the growing steps, forming $Ba_xSr_{1-x}SO_4$ solid solution terraces. Therefore, the kinetics of step advancement must depend on the supersaturation of the aqueous solution with respect to the different compositions of the $Ba_xSr_{1-x}SO_4$ solid solution.

Higgins et al. [12], have shown that the advancement of ⟨120⟩ monosteps on barite (001) surfaces can be described by means of a one-dimensional nucleation model [49–51]. According to this model, the dependence of step rate on supersaturation is given by the expression

$$v = 2bw(S-1)S^{1/2}e^{-\varepsilon/kT} \quad (3)$$

where v is the velocity of a straight step; b is the width of a kink perpendicular to the step direction (the value $b = 0.7$ nm can be used for the case of barite ⟨120⟩ steps [12]); S is the supersaturation; w is the attachment frequency of growth units at kinks; ε is the kink formation energy; k is the Boltzmann constant (1.38×10^{-23} J/K) and T is the absolute temperature.

Eq. (3) can be generalized to the case of the $Ba_xSr_{1-x}SO_4$–H_2O SS–AS system. For this purpose, it is necessary to take into account that the parameters in that equation vary with the solid and aqueous solution composition. Thus, Eq. (3) can be rewritten as

$$v(x) = 2b(x)w(x)\left[(S(x)-1)\sqrt{S(x)}\right] \cdot e^{-\varepsilon(x)/kT} \quad (4)$$

where the introduction of x in brackets denotes that the parameters are now functions of solid composition. In order to study the behaviour of Eq. (4) it is necessary to

evaluate the dependence on the solid composition of the different parameters in this equation, i.e. supersaturation, depth of the kinks on the growth steps, attachment frequency of growth units at kinks and kink formation energy. In what follows we shall discuss how to evaluate them.

Supersaturation function $S(x)$: In Section 2, it was shown that the supersaturation state of an aqueous solution with respect to the $Ba_xSr_{1-x}SO_4$ solid solution composition can be described using Eq. (2). The supersaturation in Eq. (4) is expressed in terms of saturation ratio, S. However, when the mean ionic activity of the ions in solution is considered, the following relationship between supersaturation ratio and supersaturation can be defined: $S(x) = \sqrt{\beta(x)}$. Fig. 8 shows the calculated supersaturation curves, $S(x)$, for the aqueous solutions used in the AFM growth experiments. As it can be seen, despite the $X(Ba^{2+}_{aq})$ of the solutions are very low (i.e. the solutions are very Sr-rich), supersaturation maxima correspond to intermediate $Ba_xSr_{1-x}SO_4$ solid solution compositions. This is a consequence of the significant difference between solubility products of endmembers of the celestite–barite solid solution.

The width of the kinks perpendicular to the step, $b(x)$: If we consider the $Ba_xSr_{1-x}SO_4$ solid solution as an almost ideal solid solution, a linear variation of the depth of the kinks, $b(x)$, can be assumed.

The attachment frequency of growth units at kinks, $w(x)$: The frequency of attachment of growth units into a step can be considered to depend on the solubility. This can be justified because, at a given supersaturation, the higher the solubility of a given $Ba_xSr_{1-x}SO_4$ solid solution composition the higher the concentration of growth units in the aqueous solution and, therefore, the higher the frequency of attachment. As first estimate, we can assume that the frequency of attachment is proportional to the stoichiometric solubility (Eq. (1)):

$$w(x) = w_0 K_{ss} \tag{5}$$

The kink formation energy, $\varepsilon(x)$: When the edge free energy, γ, is high, the kink formation energy, ε, can be approximated to γ [50]. Since celestite and barite are sparingly soluble compounds with high interfacial free energy, this approximation seems to be reasonable. Again, the dependence of $\varepsilon(x)$ on solid solution composition can be assumed to be linear

$$\varepsilon(x) = \gamma_{[120]_{celestite}} + (\gamma_{[120]_{barite}} - \gamma_{[120]_{celestite}})x \tag{6}$$

The values of the edge free energy of the barite and celestite steps have been estimated by Bennema and Söhnel [52]. According to these authors, the edge free energies for [120] steps are around 9.91×10^{-21} J for celestite and 1.66×10^{-21} J for barite.

Although the estimates proposed above can be questioned, their introduction in Eq. (4) will allow us to explain both the increase in step rate as the $[SrSO_4]$ concentration of the growth solution increases and the Sr-rich composition of the newly-formed terraces. Fig. 9 shows the step velocity versus $Ba_xSr_{1-x}SO_4$ solid composition calculated for the compositions of the aqueous solutions used in the AFM experiments. The maximum step velocity, in all the experiments, corresponds to Sr-rich compositions. According to these step rate distributions, the newly-grown terraces should have compositions very close to the celestite

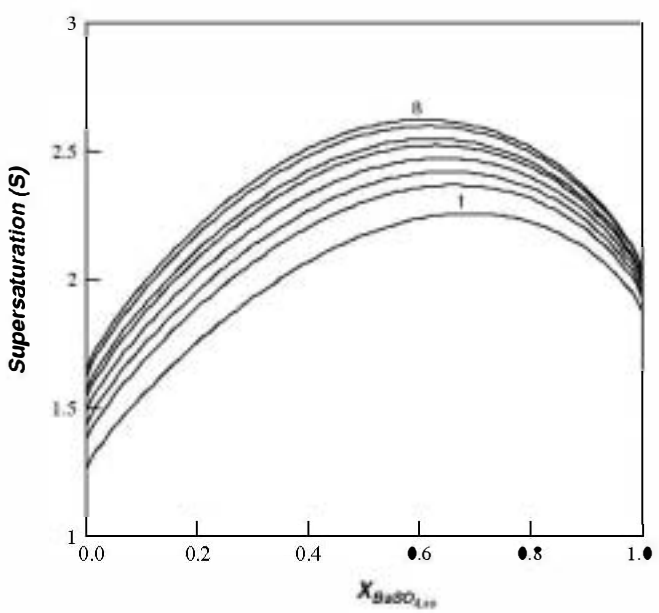

Fig. 8. Curves of supersaturation corresponding to aqueous solutions used in the AFM experiments 1 8. Note that supersaturation maxima correspond to intermediate $Ba_xSr_{1-x}SO_4$ solid solution compositions.

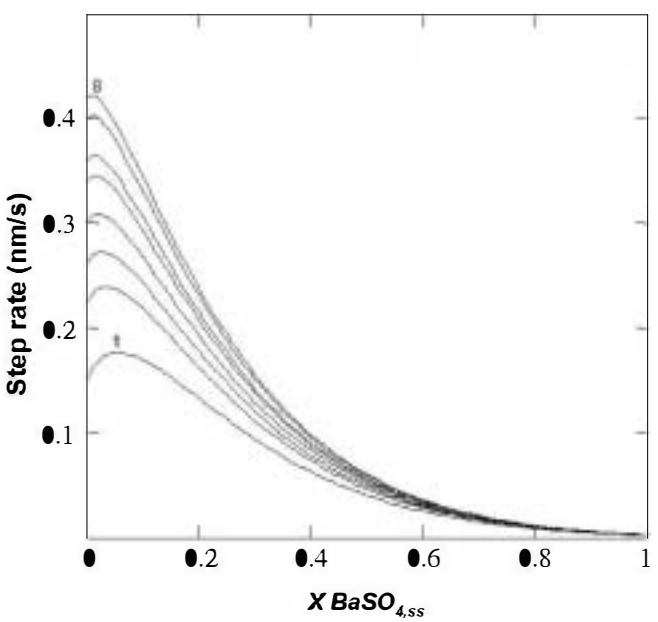

Fig. 9. Curves of step velocity as a function of the solid compositions, calculated using Eq. (4). Note that the maxima of step velocities correspond to Sr-rich compositions. (Step rates has been calculated for $w_0 = 1.7 \times 10^4$. This value provides step rates of the same order of magnitude as our experimental data).

end-member. This is in agreement with our AFM measurements.

In the generalisation of the step rate equation to the $Ba_xSr_{1-x}SO_4$–H_2O SS–AS system (Eq. (4)) the assumption that the growth of each possible solid solution composition occurs from a step edge with identical composition is implicit. However, in our AFM experiments the situation is different since the advancement of $Ba_xSr_{1-x}SO_4$ solid solution steps initiates from a pre-existent pure $BaSO_4$ step edge. Such a starting point will essentially affect the generation of kink sites. According to the one-dimensional nucleation model, the formation of kink sites is due to the attachment of growth units along the step edges, i.e. the nucleation of kinks [50,51]. One-dimensional nucleation implies the existence of an energy barrier for the attachment of growth units along the steps. In the case of $Ba_xSr_{1-x}SO_4$ steps growing in structural continuity with the pre-existent pure barite substrate, it can be expected a higher energy barrier for one-dimensional nucleation as a result of the attachment of $SrSO_4$ growth units rather than of $BaSO_4$ growth units. This is reasonable if we consider the significant differences in the first order rate constants (or frequencies) of dissociation of water molecules from the inner coordination sphere of Sr^{2+} and Ba^{2+} ions ($10^{8.7}$ s^{-1} and $10^{9.2}$ s^{-1}, respectively) [53]. In addition, a lower energy barrier for one-dimensional nucleation of $BaSO_4$ growth units is also in agreement with the so-called Paneth–Hahn–Fajans rule [54], which states that the adsorption of ions that form the least soluble salt with a given ion of the opposite sign is favoured ($BaSO_4$ in the case that we are dealing with). Thus, the direct attachment of $SrSO_4$ growth units along pure barite steps should be much less frequent than the attachment of $BaSO_4$ growth units. This seems to be in agreement with the results of the experiments in the absence of Ba (solutions 9 and 10). In these experiments, steps advancement was not observed, despite of the fact that both solutions were supersaturated with respect to pure celestite. Such behaviour indicates that the first generation of kink sites is essentially due to the attachment of $BaSO_4$ growth units along the previous barite steps, suggesting that the density of kinks on the original barite cleavage steps is much lower than during growth. In a previous work, it was also shown that, for long observation times, cleavage steps do not grow on barite (001) surfaces in contact with pure $SrSO_4$ solutions and only when the supersaturation with respect to celestite reached a value above $S = 3.9$, growth occurred by two-dimensional nucleation [7]. These observations confirm that the incorporation of $SrSO_4$ growth units into pure monomolecular barite steps is especially difficult.

AFM observations suggest that the growth kinetics of $Ba_xSr_{1-x}SO_4$ steps on barite (001) surfaces is controlled by the kink formation along the barite step edges, which at an initial stage is mainly due to the attachment of $BaSO_4$ growth units, and the incorporation of $SrSO_4$ growth units into the newly-formed kink sites. This is in agreement with the one-dimensional nucleation model.

6. Concluding remarks

1. Growth has been promoted by passing Sr–Ba–SO_4 aqueous solutions over barite (001) surfaces. Step advancement in structural continuity with the original substrate lead to the formation of terraces with $Ba_xSr_{1-x}SO_4$ composition.
2. The newly-grown terraces are clearly lower than the original barite cleavage terraces, indicating the extensive incorporation of Sr^{2+} into the barite structure during growth. However, our measurements have shown that the decrease in terrace height is higher than expected, presumably as a consequence of a relaxation of the structure of the new terraces.
3. AFM measurements show a non-linear dependence of the step rates on [$SrSO_4$] concentration. While for solutions with [$SrSO_4$] concentrations below about 1150 μmol/l, step velocities are low and independent of the solution concentration, for solutions with [$SrSO_4$] concentrations higher than 1150 μmol/l, step velocities rapidly increase with the [$SrSO_4$] concentration in the solution.
4. The step rate equation based on a one-dimensional nucleation model has been generalised to the $Ba_xSr_{1-x}SO_4$–H_2O SS–AS system (Eq. (4)). This allowed us to provide a general and qualitative explanation of both the kinetic behaviour of the $Ba_xSr_{1-x}SO_4$ steps and the compositional characteristics of the newly-formed terraces. In addition, AFM observations indicate that the kinetics of step advancement is controlled by the nucleation of kinks along step edges by growth unit incorporation and the attachment of growth units into the kink sites. The observed growth behaviour suggests that the attachment of $BaSO_4$ growth units mainly controls the generation of kinks along steps. Nevertheless, a more quantitative description of monostep kinetics in the $Ba_xSr_{1-x}SO_4$–H_2O SS–AS system will require further experimental AFM work on both barite and celestite surfaces.

Acknowledgements

Ch. YuHang acknowledges the Agencia Española de Cooperación for a research grant. N. Sánchez-Pastor acknowledges the Spanish Ministry of Education and Science (Project Number: BTE2002-00325) for a FPI research grant. A. Asenjo and C.M. Pina acknowledge Spanish Ministry of Education and Science for financial support ("Ramón y Cajal" program). The barite sample (MNCN 7986) was kindly provided by Begoña Sánchez and Javier Garcia-Guinea (Museo Nacional de Ciencias Naturales, Spain).

References

[1] A.J. Gratz, P.E. Hillner, J. Cryst. Growth 129 (1993) 789.
[2] C.M. Pina, D. Bosbach, M. Prieto, A. Putnis, J. Cryst. Growth 187 (1998) 119.

[3] D.G. Bokern, W.A.C. Ducker, K.A. Hunter, K.M. McGrath, J. Cryst. Growth 246 (2002) 139.
[4] S.J. Freij, G.M. Parkinson, M.M. Reyhani, J. Cryst. Growth 260 (2004) 232.
[5] S.J. Freij, A. Putnis, J.M. Astilleros, J. Cryst. Growth 267 (2004) 288.
[6] J.M. Astilleros, C.M. Pina, L. Fernández-Díaz, A. Putnis, Surf. Sci. 545 (2003) 767.
[7] N. Sánchez-Pastor, C.M. Pina, J.M. Astilleros, L. Fernández-Díaz, A. Putnis, Surf. Sci. 581 (2005) 225.
[8] G. Jordan, W. Rammensee, Geochim. Cosmochim. Acta 60 (1996) 5055.
[9] Y.G. Kuznetsov, J. Konnert, A.J. Malkin, A. McPherson, Surf. Sci. 440 (1999) 69.
[10] T.A. Land, J.J. De Yoreo, J.D. Lee, Surf. Sci. 384 (1997) 136.
[11] D. Bosbach, G. Jordan, W. Rammensee, Eur. Micro. Anal. (1994) 15.
[12] S.R. Higgins, D. Bosbach, C.M. Eggleston, K.G. Knauss, J. Phys. Chem. B 104 (2000) 6978.
[13] T.A. Land, T.L. Martin, S. Potapenko, G.T. Palmore, J.J. De Yoreo, Nature 399 (1999) 442.
[14] J.J. De Yoreo, T.A. Land, L.N. Rashkovich, T.A. Onischenko, J.D. Lee, O.V. Monovskii, N.P. Zaitseva, J. Cryst. Growth 182 (1997) 442.
[15] K.J. Davies, P.M. Dove, J.J. DeYoreo, Science 290 (2000) 1134.
[16] N. Kubota, M. Yolota, J.W. Mullin, J. Cryst. Growth 182 (1997) 86.
[17] J.M. Astilleros, C.M. Pina, L. Fernández-Díaz, M. Prieto, A. Putnis, Chem. Geol. 225 (2006) 322.
[18] R.A. Berner, Geochim. Cosmochim. Acta 39 (1975) 489.
[19] W.J.P. van Enckevort, A.C.J.F. van den Berg, J. Cryst. Growth 183 (1998) 441.
[20] N. Cabrera, D.A. Vermilyea, in: R.H. Doremos, B.W. Roberts, D. Turnbull (Eds.), Growth and Perfection of Crystals, Chapman & Hall, London, 1958, p. 393.
[21] K. Sangwal, I. Owczarek, J. Cryst. Growth 129 (1993) 640.
[22] W.J.P. van Enckevort, C.J.F. van den Berg, K.B.G. Kreuwel, A.J. Derksen, M.S. Couto, J. Cryst. Growth (1996) 156.
[23] N. Kubota, J.W. Mullin, J. Cryst. Growth 152 (1995) 203.
[24] Y. Yoshioka, T. Matsui, M. Kasuga, T. Irisawa, J. Cryst. Growth 198/199 (1999) 71.
[25] L.E. Wasylenki, P.M. Dove, D.S. Wilson, J.J. De Yoreo, Geochim. Cosmochim. Acta 69 (2005) 3017.
[26] F. Lippmann, N. Jb. Mineral. Abh. 139 (1) (1980) 1.
[27] P.D. Glynn, E.J. Reardon, Am. J. Sci. 290 (1990) 164.
[28] M. Prieto, A. Putnis, L. Fernández-Díaz, Geol. Mag. 130 (1993) 289.
[29] C.M. Pina, M. Enders, A. Putnis, Chem. Geol. 168 (2000) 195.
[30] P. Risthaus, C.M. Pina, D. Bosbach, U. Becker, A. Putnis, Ber. Dtsch. Min. Ges. 10 (1998) 237.
[31] C.M. Pina, U. Becker, P. Risthaus, D. Bosbach, A. Putnis, Nature 395 (1998) 483.
[32] D. Bosbach, C. Hall, A. Putnis, Chem. Geol. 151 (1998) 143.
[33] N. Sánchez-Pastor, C.M. Pina, L. Fernández-Díaz, J.M. Astilleros, Surf. Sci. 600 (2006) 1369.
[34] R.J. Hill, Can. Miner. 15 (1977) 522.
[35] M.A. Simonov, S.I. Troyanov, Vestn. Mosk. Uni. 4 (1987) 77.
[36] F. Lippmann, Bull. Miner. 105 (1982) 273.
[37] J.S. Hanor, Am. Miner. 53 (1968) 1215.
[38] E. Brower, J. Renault, New mexico state bureau of mines and mineral resources, Circular No. 116 (1971).
[39] S.D. Malinin, V.S. Urusov, Geokhimiya 9 (1983) 1324.
[40] A.R. Felmy, D. Rai, D.A. Moore, Geochim. Cosmochim. Acta 57 (1993) 4345.
[41] U. Becker, A. Fernández-González, M. Prieto, R. Harrison, A. Putnis, Phys. Chem. Miner. 27 (2000) 291.
[42] C.W. Blount, Am. Miner. 62 (1977) 942.
[43] E.J. Reardon, D.K. Armstrong, Geochim. Cosmochim. Acta 51 (1987) 63.
[44] M. Prieto, A. Fernández-González, L. Fernández-Díaz, Geochim. Cosmochim. Acta 61 (1997) 3383.
[45] J.M. Astilleros, C.M. Pina, L. Fernández-Díaz, A. Putnis, Geochim. Cosmochim. Acta 66 (2002) 3177.
[46] D.L. Parkhurst, C.A.J. Appelo, User's guide to PHREEQC (version 2). A computer program for speciation, batch-reaction, one-dimensional transport, and inverse geochemical calculations (US Geological Survey Water-Resources Investigations Report 99-4259, 2000) p. 312.
[47] P. Hartman, W.M.M. Heijnen, J. Cryst. Growth 63 (1983) 261.
[48] P. Hartman, C.S. Strom, J. Cryst. Growth 97 (1989) 502.
[49] V.V. Voronkov, Sov. Phys. Crystallogr. 15 (1970) 8.
[50] J. Zhang, G.H. Nancollas, J. Cryst. Growth 106 (1990) 181.
[51] F.C. Frank, J. Cryst. Growth 22 (1974) 233.
[52] P. Bennema, O. Söhnel, J. Cryst. Growth 102 (1990) 547.
[53] A.E. Nielsen, J. Cryst. Growth 22 (1984) 289.
[54] K. Horovitz, F. Paneth, Z. Physik. Chem. 89 (1915) 513.